Available online at www.eccomasproceedia.org
Eccomas Proceedia COMPDYN (2023) 112-126

ECCOMAS
Proceedia

COMPDYN 2023
9th ECCOMAS Thematic Conference on
Computational Methods in Structural Dynamics and Earthquake Engineering
M. Papadrakakis, M. Fragiadakis (eds.)
Athens, Greece, 12-14 June 2023

SEISMIC RETROFITTING OF PRECAST INDUSTRIAL BUILDINGS THROUGH ENERGY DISSIPATION DEVICES

Davide Bellotti[1], Francesco Cavalieri[1], and Roberto Nascimbene[2]

[1] European Centre for Training and Research in Earthquake Engineering (EUCENTRE)
Via Ferrata 1, 27100 Pavia, Italy
e-mail: {davide.bellotti,francesco.cavalieri}@eucentre.it

[2] University School for Advanced Studies (IUSS)
Palazzo del Broletto, Piazza della Vittoria 15, 27100 Pavia, Italy
e-mail: roberto.nascimbene@iusspavia.it

Abstract

Seismic retrofitting strategies encompassing the use of dissipation devices can effectively yield a performance enhancement and an extension of the nominal service life of reinforced concrete precast industrial buildings. This work investigates the behaviour of two energy dissipation devices designed for retrofit of precast buildings, namely a friction rotation damper for beam-to-column connections and a bracing system with dissipative sacrificial elements, with the aim of testing their effectiveness in improving the seismic response of this construction system. The advantages deriving from the use of such devices, which are typically coupled with elements preventing joint sliding, include the reduction of global lateral displacements and resisting forces in the main structural elements, the increase of the building's lateral strength, as well as their replaceability after a seismic event. Considering a single-storey industrial building as a case study, a comparative analysis of the seismic response of the structure before and after the retrofit with the two proposed devices was undertaken. Two three-dimensional numerical models of the building, with and without the retrofit, were created in OpenSees and first subjected to nonlinear static (pushover) analyses in both the main directions. Then, a number of nonlinear dynamic analyses were carried out at increasing seismic intensity levels, within a multiple-stripe analysis framework. With reference to two limit states, the obtained results provided reassurance on the efficacy of the proposed solutions in improving the seismic performance of existing and new precast industrial buildings.

Keywords: Friction rotation damper, Braces, Dissipative sacrificial elements, Pushover, Multiple-stripe analysis (MSA), Dissipated energy.

ISSN:2623-3347
Peer-review under responsibility of the organizing committee of COMPDYN 2023.
doi: 10.7712/120123.10391.21125

1 INTRODUCTION

Italian reinforced concrete (RC) precast industrial buildings, especially those not specifically designed to resist seismic actions, suffered from extensive damage following the recent earthquakes that struck Italy, namely Abruzzo 2009, Emilia-Romagna 2012 and Central Italy 2016-2017 (see e.g. Praticò et al., 2022 [1]). The seismic response of these buildings can be generally improved by imposing the dissipation of an appropriate amount of energy. In the last decade, a large body of literature has been devoted to the development and the application of dissipation devices that can be used for precast structures, to enhance their seismic performance and extend their nominal service life. The practical issues that have been considered include the potential to use the devices for both existing and new precast structures, the possibility to inspect the devices from close up, the replaceability after a seismic event, the dry installation without the use of mortar, and the compatibility with the techniques adopted for the construction of typical precast buildings, for instance in the case of structures with monolithic columns and pin-ended beams (Belleri et al., 2010) [2]. The devices typically employed for these structures can dissipate energy through friction or by hysteresis and may be combined with elements having the function to increase the initial stiffness; in this way, they prevent or mitigate the second order effects and avoid excessive displacements at the serviceability limit state, which often drive the design of flexible structures.

While several works in the current literature explored the feasibility of energy dissipative cladding panel connection systems, the focus in this work is on dissipation devices designed for beam-to-column connections of precast industrial buildings, as well as dissipative bracing systems. Several researchers to date proposed retrofitting solutions that are applicable to frictional beam-to-column connections (e.g. Martinelli and Mulas, 2010 [3], Santagati et al., 2012 [4], Pollini et al., 2013 [5], Belleri et al., 2017 [6], Magliulo et al., 2017 [7], Hu et al., 2020 [8], Belleri and Labò, 2021 [9], Bai et al., 2022 [10], Quaglini et al., 2022 [11], Sonda and Pollini, 2023 [12]), or that make use of dissipative braces (e.g. Dal Lago et al., 2021 [13]). The goal of this paper is to provide an additional contribution to this relevant field, by testing the effectiveness of energy dissipation devices in improving the seismic response of precast industrial buildings. With reference to a single-storey case study building, a comparative analysis was undertaken on the seismic response of the structure before and after the retrofit with two proposed dissipation devices, namely a friction rotation damper for beam-to-column connections and a bracing system with dissipative sacrificial elements. The advantages deriving from the use of such devices include not only the reduction of global lateral displacements and resisting forces in the main structural elements, and the increase of the building's lateral strength, but also their replaceability after a seismic event. Two three-dimensional numerical models of the case study building, with and without the retrofit, were created in OpenSees (McKenna et al., 2000) [14] and first subjected to nonlinear static (pushover) analyses in both the main directions. Then, a number of nonlinear dynamic analyses (NDAs) were carried out at increasing seismic intensity levels, within a multiple-stripe analysis (MSA) framework (Jalayer and Cornell, 2009) [15]. A state-of-the-art toolbox for record selection was used to implement the conditional spectrum (CS) method [16] and select, at each level, both horizontal components of 20 natural spectrum-compatible recordings, extracted from the Engineering Strong Motion (ESM) database [17]. The average spectral acceleration (AvgSa), which has been shown to be reasonably efficient for building response prediction, was adopted as the conditioning intensity measure (IM). The results were produced in terms of pushover curves and demand-over-capacity ratio curves, the latter being assessed within NDAs and with reference to two limit states, namely the Usability Preventing Damage (UPD) and the Global Collapse (GC).

This work is part of a more comprehensive research endeavour by the authors, prompted by the relevance of sustainability issues related to the reduction of economic and environmental impacts (in terms of earthquake-induced losses) allowed by the retrofit; in particular, the research aims to explore the beneficial effects of dissipation devices to the life cycle seismic performance of precast structures, as well as their own life cycle environmental impact.

2 CASE STUDY BUILDING AND ADOPTED DISSIPATION DEVICES

The case study considered for this endeavour, depicted in Figure 1, is a single-storey precast structure representative of the Italian construction period of the '70s, located in Naples and designed on the base of gravity loads only. The geometry consists of a single span with total plan size of 20 × 54 m^2. The columns, with a 0.35 × 0.35 m^2 cross-section and a 6 m height, are installed into socket foundations filled with concrete. The prestressed main beams in the transverse (x) direction feature a span length of 20 m and a double slope of 10% inclination; their I-section has variable height (max 1.82 m at midpoint) and thickness (min 0.08 m at midpoint). The secondary beams (or girders) in the longitudinal (y) direction are 6 m long with a tee cross-section. The connections of the main beams to the columns only rely on friction and are characterised by the presence of neoprene pads on the column top allowing for beam seating. On the other hand, the girders are fastened to the columns by steel dowels. The roof is composed of double-tee prestressed elements, rigidly fastened to the main beams by reinforcement stirrups protruding from the beams, additional steel bars between the elements and a finishing concrete casting. The external closure is present on all sides of the building and is constituted of masonry infill panels, of the type called Italian "double-UNI", creating a ribbon window of a 1.5 m height.

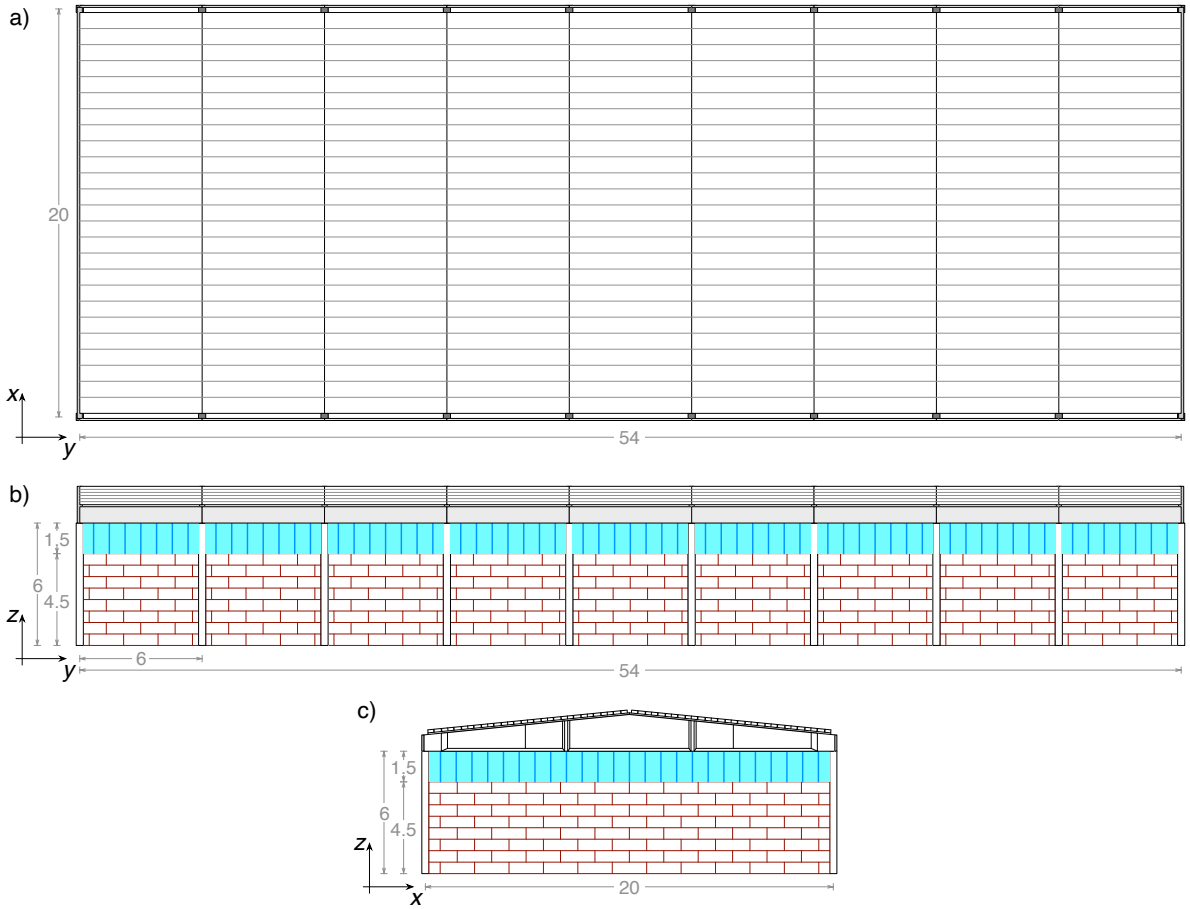

Figure 1: a) Top, b) side and c) frontal view of the case study building (Units: m).

2.1 Dissipation devices

The first dissipation device considered herein is a friction rotation damper (see Figure 2), conceived to be applied at beam-to-column connections. The device is able to dissipate energy (thus increasing the system damping) through the friction generated by the relative rotation of steel plates with interposed brass discs. The interposition of brass discs, softer than the connected steel plates, guarantees smoothness during relative rotations (Belleri et al., 2017) [6]. The increase of the device activation moment is accomplished by incrementing the number of sliding surfaces (four in Figure 2b). The steel plates are fixed to the mounting frame by bolts placed in slotted holes, thus transferring the external tightening force to the brass discs. Cup springs are introduced on the main bolt for a better control of the tightening load acting on the brass discs. For each beam-to-column connection, the device works in a three-hinge scheme, where sliding surfaces are applied only at one hinge, whilst the remaining two hinges are left free to rotate. In the current study, this first retrofitting solution encompasses the use of the rotation damper coupled with steel profiles and passing holes hosting steel pins, which allow for relative rotations but prevent joint sliding (see Figure 2a). Also, given the presence of secondary beams, with no specific structural function, in the perimeter portal frames along the longitudinal direction, it was decided to install the rotation dampers only at the beam-to-column frictional connections in the ten portal frames that include the main beams, along the transverse direction. The size of the devices allows some clearance between them and the masonry infills, which are thus left intact.

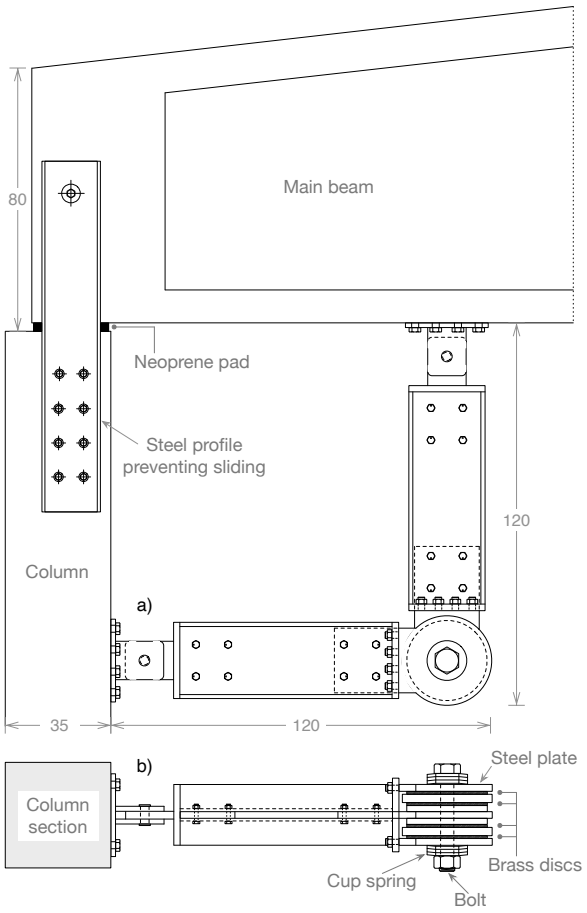

Figure 2: a) Side and b) bottom view of the adopted friction rotation damper applied at beam-to-column connections (Units: cm).

The second dissipation solution adopted in this work entails the use of non-traditional diagonal steel braces, characterised by the inclusion of dissipative sacrificial elements, as well as the presence of a junction in the middle, which allows the upper and lower portions of the braces to be off-axis (Resilio system, 2017) [18]. This system is able to channel the ingoing seismic energy towards predefined points in the vicinity of the junction, where the steel sacrificial elements are located (see Figure 3): the latter are pushed in the nonlinear field and dissipate energy by material hysteresis of steel, thus preserving the rest of the structure. A crucial property of this system is its immediate activation during an earthquake, something that prevents the occurrence of strong bending moments at the base of the columns. The elements may be easily replaced after a seismic event. Moreover, the global static scheme of the structure remains unchanged. In the current study, given the relevant width (i.e. 20 m) of the portal frames along the transverse direction, the braces are installed only along the longitudinal direction, and in particular within the central bay of the perimeter portal frames (see Figure 1b). The braces are connected to the bottom and the top portions of the columns, thus occupying the entire clearance below the girders: consequently, the central field of masonry infill must be removed and the glazing of the correspondent ribbon window dismounted; then, after the retrofitting intervention, lightweight infills made of green or sustainable materials are put in place only for closure purposes, and the glazing is just remounted.

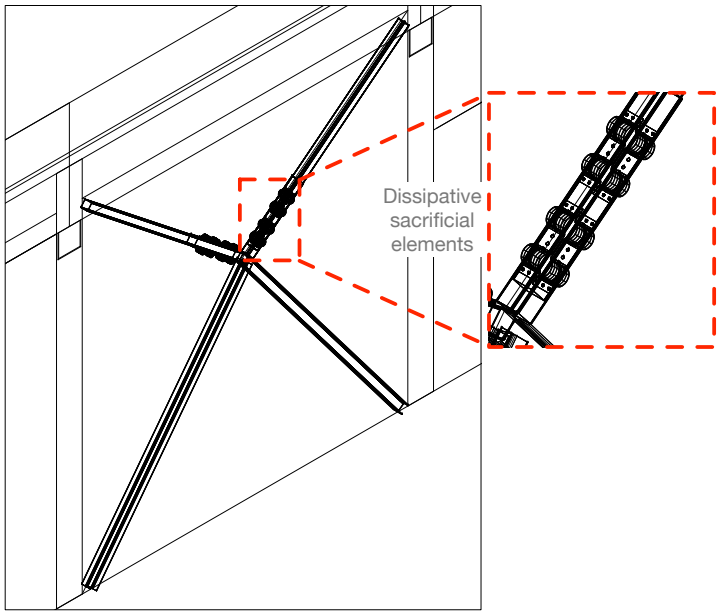

Figure 3: Diagonal steel braces, with a close-up on the dissipative sacrificial elements.

3 MODELLING ASSUMPTIONS

Two three-dimensional numerical models of the case study building, with and without the retrofit, were created in OpenSees. In both building models, a concentrated plasticity approach with a plastic hinge at the base of the columns was used to describe the global structural nonlinear behaviour; in the adopted model, the stiffness of the entire element is obtained by connecting in series the stiffness of the rotational spring and the one of the column element. The plastic hinge model was defined using the *ModIMKPeakOriented* material, as implemented in OpenSees, whose mechanical parameters were assigned according to Bosio et al. (2023) [19]. A rigid link was introduced on top of each column so as to properly account for the eccentricity between the column and the main beam axis. The beam-to-column frictional connections for the main beams were modelled by means of the *flatSliderBearing* element of OpenSees, which

allows for the translation in both the main horizontal directions at the attainment of the friction force. The latter was computed following the Coulomb model, in which the friction coefficient was evaluated according to the model proposed by Magliulo et al. (2011) [20] for neoprene-concrete friction, as a function of the normal stress acting on the sliding surface. On the other hand, pinned connections (i.e. pure hinges) were introduced to model the beam-to-column dowel connections for the girders. The properties of the roof system, as described in Section 2, justify the adopted assumption of rigid diaphragm for the roof: in particular, the roof elements were explicitly introduced as elastic elements, rigidly connected to the main beams. The masonry infills were modelled following the work by Liberatore et al. (2018) [21], based on the equivalent strut approach. With reference to the Italian "double-UNI" infill masonry, with a thickness of 24 cm, the stress and strain values provided by Bosio et al. (2023) [19] were adopted herein. Such values were introduced in OpenSees using the *Concrete01* material. For each field of masonry infill, two *twoNodeLink* elements with the latter material and embedding the infill's mass were employed to model two diagonal compression-only connecting struts. Given the presence of a ribbon window on all sides of the case study building, an additional lumped plastic hinge was introduced, through a *zeroLength* element, at the intersection between the upper end of the equivalent strut and the column, so as to model the behaviour of the upper squat part of the column (also called short column hereafter), failing in flexure.

The friction rotation dampers were introduced in the retrofitted structural model adopting the following strategy. First, in order to simulate the presence of steel profiles that allow for relative rotations but prevent joint sliding along both the main directions, the beam-to-column frictional connections, modelled by means of *flatSliderBearing* elements in the unretrofitted model, were replaced with pinned connections; it is important to note that rotations are allowed only in the in-plane (transverse) direction and prevented in the out-of-plane direction, as well as about the axis of the main beams. Then, within the three-hinge scheme described above, the two lateral hinges that are left free to rotate were modelled as pinned connections by means of *zeroLength* elements with sufficiently low rotational stiffness. On the other hand, the central hinge where sliding surfaces are applied was introduced in OpenSees as a *zeroLength* element characterised, in the rotational degree of freedom of interest, by a rigid-plastic behaviour: this choice is consistent with the experimental hysteretic behaviour of dampers with different values of slip force (analogous to activation moment) presented by Morgen and Kurama (2008) [22], as well as with the findings of several other studies (e.g. Bagheri et al., 2015 [23]). In particular, using the *MultiLinear* material of OpenSees, an elastic-perfectly plastic behaviour was assigned, with "large" initial stiffness and moment capacity equal to 40 kNm: the latter value was selected for this application among the three values of activation moment considered by Santagati et al. (2012) [4], namely 40, 80 and 120 kNm, related to the properties of the cup springs (see Figure 2b). The three *zeroLength* elements are connected to each other, as well as to the column and the main beam, by rigid links. It is noteworthy that the horizontal rigid link connecting one of the lateral hinges to the column, is attached to the upper node of the *zeroLength* element (i.e. the plastic hinge) introduced at the base of the short column adjacent to the ribbon window: with this configuration, the formation of the plastic hinge and the consequent occurrence of the "squat column" effect is somehow hampered, though not prevented.

Coming to the second retrofitting solution, firstly the *twoNodeLink* elements that model masonry infills in the central bay of the perimeter portal frames along the longitudinal direction were removed; they were not replaced with other elements, under the assumption that lightweight infills only serve the purpose of closing the internal space and do not contribute to the lateral stiffness of the structure. The junction was modelled with one central node plus four additional lateral nodes along the directions of the upper and lower portions of the braces; four *zeroLength* elements with very low rotational stiffness (i.e. pure hinges) were then introduced

between the deriving four couples of nodes. The lower portions of the braces were modelled as elastic elements having the properties of HEA200 profiles with S275 steel, with one end node attached to the correspondent node of the junction, and the second end node attached to the base node of the columns (i.e. beneath the base plastic hinges). On the other hand, the entire upper portions of the braces were modelled with two *twoNodeLink* elements, representing the dissipative sacrificial elements, with one end node attached to the correspondent node of the junction, and the second end node attached to a *zeroLength* element (a pure hinge), itself connected to the lower node of the rigid link introduced on top of each column. Taking as benchmark the experimental results provided by the manufacturer, related to a single sacrificial element of class 60, constituted of 60 × 4 mm S355 steel lamellas, an OpenSees *BoucWen* hysteretic material with stiffness and strength degradation was calibrated, disregarding the pinching behaviour for simplicity (see Figure 4a). To model the presence of four sacrificial elements arranged according to the scheme in Figure 3, four identical calibrated *BoucWen* materials were created, each couple was combined in parallel (using the *Parallel* material of OpenSees) and then the two derived parallel materials were combined in series (through the *Series* material of OpenSees), obtaining a material with an axial force capacity of nearly 30 kN; subsequently, the *MinMax* command of OpenSees was employed in order to simulate the failure of the system when the displacement demand falls below or above certain minimum and maximum threshold values, the latter being fixed at -0.06 m and 0.06 m herein, based on the experimental behaviour.

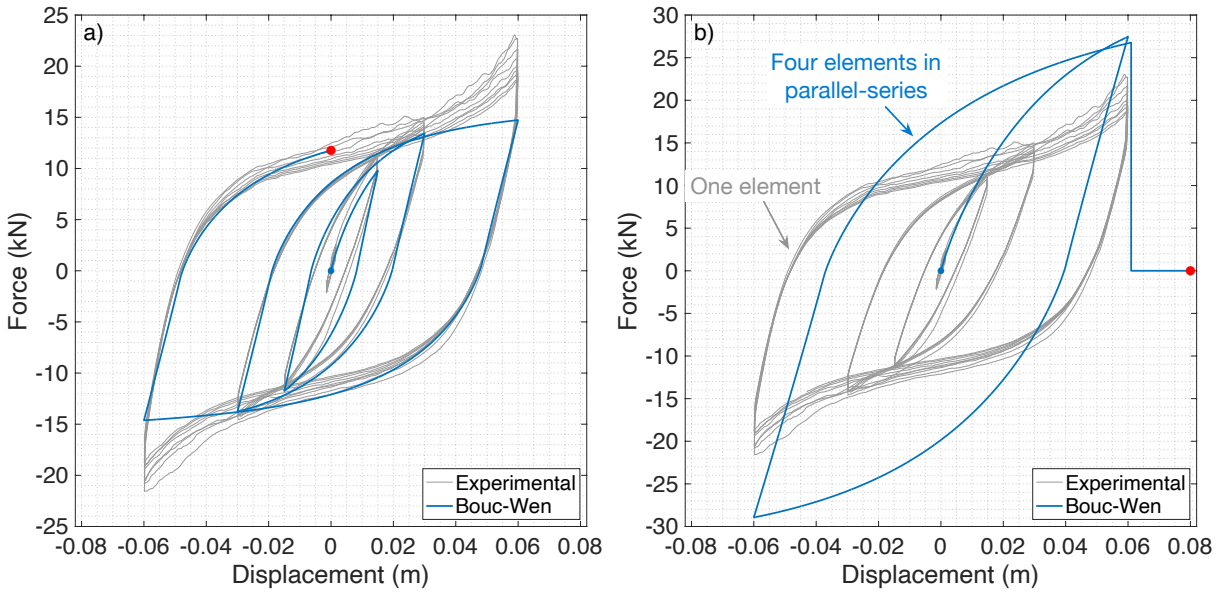

Figure 4: Cyclic behaviour a) of the *BoucWen* hysteretic material calibrated against experimental results, and b) of four identical *BoucWen* materials combined in parallel-series, with use of the *MinMax* command; the experimental hysteresis curve related to a single sacrificial element is also displayed, in grey, for reference.

The resulting material, whose cyclic behaviour is shown in blue in Figure 4b, was finally assigned to each *twoNodeLink* element along its axial direction, whilst a rigid elastic behaviour was applied in the other directions. In Figure 4b, the experimental hysteresis curve related to a single sacrificial element, which is actually the same curve displayed in Figure 4a, is also reported, in grey, for reference, to readily gather the increase in stiffness and axial force capacity granted by the parallel arrangement of each couple, leading to equal strains and additive stresses and stiffnesses. The numerical model featuring both the adopted retrofitting solutions is characterised by an increased global stiffness, reflected in a reduction of the fundamental period, belonging to a purely translational mode along the *x*-direction for both models, from 1.45 s to

0.45 s: this is mainly caused by the introduction of the friction rotation dampers and the pinned connections (in place of the beam-to-column frictional ones), the latter leading the model to exhibit a different static scheme with respect to the unretrofitted case.

4 ANALYSES AND RESULTS

This Section presents the results of the nonlinear static and dynamic analyses carried out along both the main directions, on both the unretrofitted and retrofitted models. Given the regularity in plan of the building, confirmed by the modal analysis and the presence of purely translational modes, as well as by the dynamic response (see Section 4.2), both models behave independently along the two directions: consequently, the two adopted retrofitting solutions play a role only along the direction in which they are applied, namely the transverse direction for the rotation dampers and the longitudinal direction for the diagonal braces. However, it has to be noted that the pinned connections representing steel profiles coupled with rotation dampers, introduced along the transverse direction, do provide a stiffening effect also along the longitudinal direction, as will be highlighted in Section 4.1.

4.1 Pushover analyses

It is noteworthy that the employed dissipation devices, like any other device of the same type, can dissipate the ingoing seismic energy only in dynamic conditions; therefore, with static analyses it is only possible to capture the increase in lateral stiffness, strength and ductility due to the installation of the devices, not their dissipation capabilities.

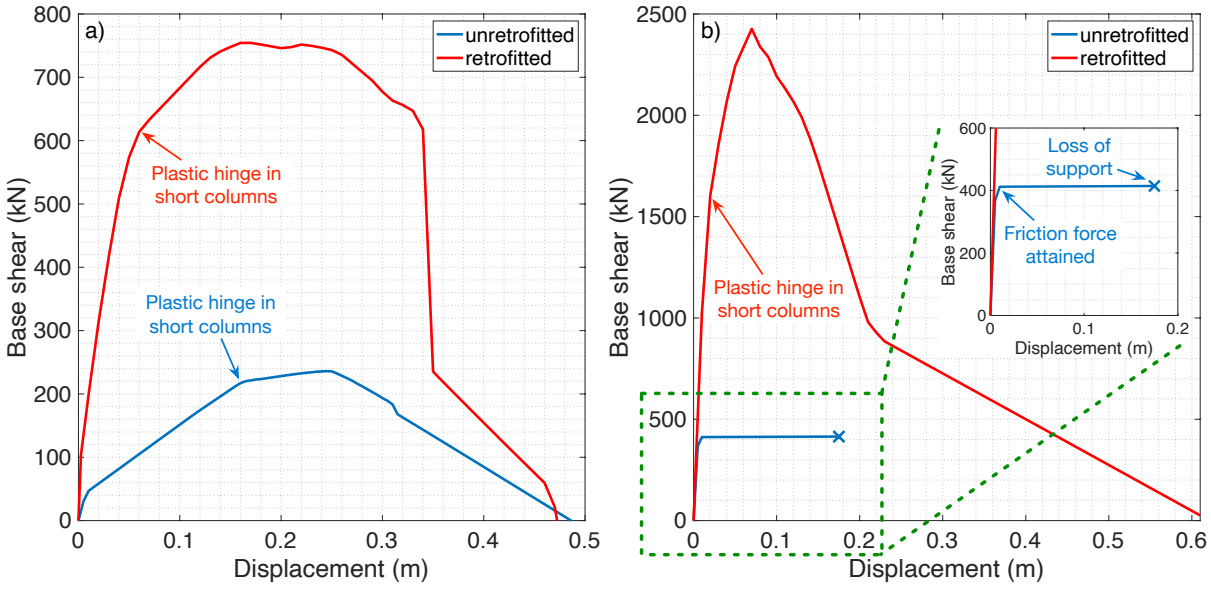

Figure 5: Results of the nonlinear static analyses for both the unretrofitted and retrofitted models, along a) the transverse (x) direction, and b) the longitudinal (y) direction, with close-up on the blue curve for the unretrofitted model.

From the pushover curves along the transverse direction (see Figure 5a), it is readily gathered that the unretrofitted structure (curve in blue) has a quite low capacity along the transverse direction, owing to the occurrence of the "squat column" effect: a plastic hinge, indicated by a change of slope in the pushover curve, is formed in the short columns adjacent to ribbon windows, only at the four corner columns that enclose infills. In the retrofitted structure, the "squat column" effect does still occur, although for a much higher base shear value (curve in red).

However, thanks to the presence of a total of 20 rotation dampers that can withstand a moment capacity of 40 kNm, as well as steel profiles preventing joint sliding, the building exhibits a significant (nearly fourfold) increase in lateral stiffness and strength.

Coming to the longitudinal direction, Figure 5b shows that the unretrofitted model (curve in blue) has a base shear limited to a value of around 400 kN, due to the attainment of the friction force in the frictional beam-to-column connections: in the latter condition, the pushover curve becomes flat, indicating that the mean beams freely slide until loss of support. On the other hand, the retrofitted building exhibits an increased lateral stiffness and a much larger resistance (curve in red), as expected. It was observed that the latter increase in lateral resistance is mainly due to the presence, in the ten portal frames along the transverse direction, of pinned connections preventing rotations about the axis of the main beams (see Section 3): the relevant role of the diagonal steel braces embedding the Resilio devices will be much better highlighted by looking at the dynamic behaviour (see Section 4.2). It is finally interesting to note that in the retrofitted model, given that the masonry infills do not collapse and the lower (main) parts of the columns do not yield, the "squat column" effect occurs again, with the formation of a plastic hinge (indicated by a change of slope in the pushover curve) in the short columns adjacent to ribbon windows.

4.2 Nonlinear dynamic analyses

As already introduced above, both the unretrofitted and retrofitted models in OpenSees were also subjected to nonlinear dynamic analyses in the two main directions, within a MSA framework. According to the latter, multiple levels of intensity, or stripes, are considered, and for each of them a number of NDAs are carried out using a suite of records, different for each stripe, all scaled to the same IM level (IML). This allows obtaining the demand values in terms of one or more engineering demand parameter (EDPs); then, adopting a deterministic value for the EDP capacity, it is possible to retrieve the demand-over-capacity (D/C) ratio curves. The conditioning IM selected for MSA was chosen to be AvgSa, defined as the geometric mean of spectral acceleration values at a set of periods of interest. As suggested by Kohrangi et al. (2017) [24], who proposed a version of the CS-based record selection conditioned on AvgSa, ten equally spaced periods were considered in the $0.2 \cdot T_1$ to $1.5 \cdot T_1$ range, where T_1 is the fundamental period of the building. In order to apply the same selected records to both the unretrofitted and retrofitted models, which are characterised by different fundamental periods (1.45 s and 0.45 s, respectively), it was herein decided to select as T_1 a value slightly higher than the mean of the two periods, namely 1.1 s, entailing a [0.22 s – 1.65 s] period range; the latter i) includes the third period (0.34 s) of the retrofitted model, belonging to a purely translational mode along the *y*-direction, and ii) in general allows covering higher mode response and period elongation for both models. Record selection was undertaken with a dedicated toolbox, namely EzGM (see Ozsarac, 2020 [25], Ozsarac et al. 2021 [26]), which calls the OpenQuake engine (Pagani et al., 2014) [27] to perform probabilistic seismic hazard analysis (PSHA) calculations. Records were selected according to the exact CS, in which all the causative scenarios are incorporated in the generation of the target conditional spectrum. The ground motion prediction equation (GMPE) by Boore et al. (2014) [28] and the spectral ordinate correlation model by Baker and Jayaram (2008) [29] were adopted. The selection was carried out with reference to the Naples site and soil type C, the latter representing an averagely dense soil with a time-averaged shear wave velocity in the upper 30 m, $V_{S,30}$, ranging between 180 and 360 m/s, according to EC8 (CEN, 2004) [30]. Eight increasing levels (i.e. the stripes) of AvgSa (0.017, 0.078, 0.119, 0.191, 0.255, 0.331, 0.449, 0.549 g), corresponding to the return periods (T_R) of 10, 50, 100, 250, 500, 1000,

2500, 5000 years, were considered within MSA: at each of them, both horizontal components of 20 natural spectrum-compatible recordings were extracted from the ESM database [17].

For the unretrofitted model, two EDPs were evaluated in the dynamic analyses. The first one is the maximum (in time) absolute value of the column drift in both horizontal directions. It is noted that the recorded values of this EDP include additional displacements occurring in the upper part of the building, caused by the possible formation of a plastic hinge in the short columns adjacent to ribbon windows. The second EDP is the maximum (in time) absolute value of the relative displacement between the beam ends and the columns, or in other words, the relative displacement of the frictional beam-to-column connections, in both horizontal directions. Clearly, for the retrofitted model, only the first EDP was actually evaluated, given that joint sliding is prevented thanks to the presence of pinned beam-to-column connections in the ten portal frames along the transverse direction.

With a view to conduct a sanity check on the modelling effort of the two employed dissipation devices and to gain insight into their dynamic responses, other quantities, in addition to the above-mentioned EDPs, were recorded in the OpenSees dynamic analyses. The moment-rotation (hysteresis) curves of the 20 *zeroLength* elements with *MultiLinear* material modelling the friction rotation dampers are shown in Figure 6a. The latter displays the responses related to one selected recording within IML #5 (T_R = 500 yr). The friction dampers being characterised by a rigid-plastic behaviour, it is not surprising that, for several of the 20 devices, the activation moment of 40 kNm is attained for a medium intensity recording that yields relatively low rotation values; this feature allows for the deployment of wide frictional hysteresis loops, which provide a clear indication of the amount of energy dissipated due to friction.

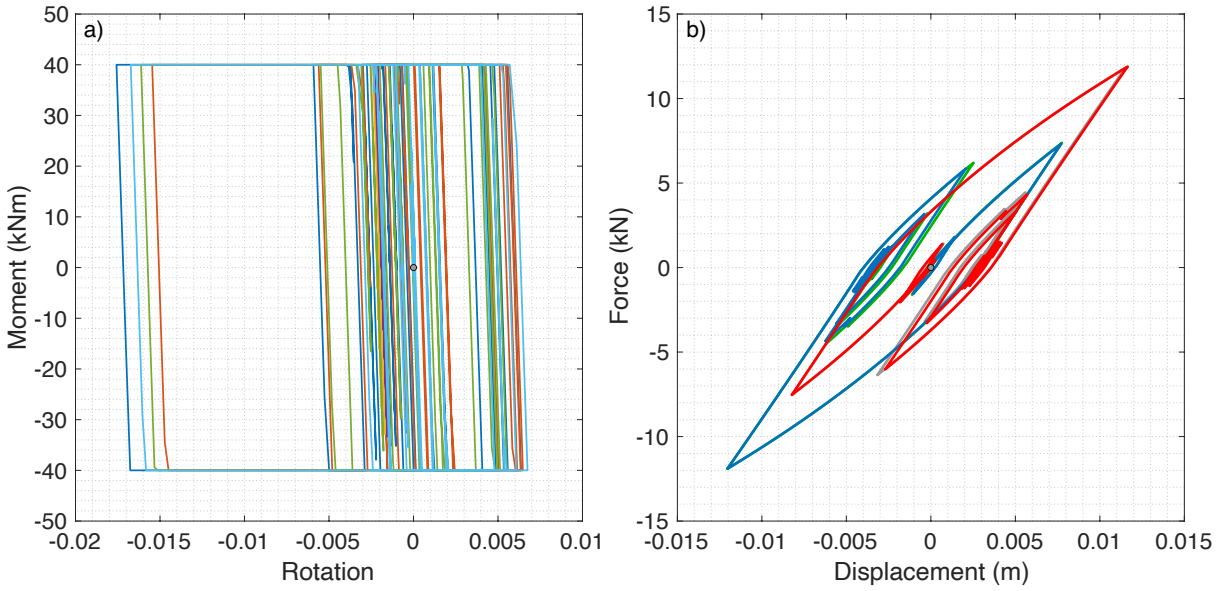

Figure 6: a) Moment-rotation hysteresis curves for the 20 *zeroLength* elements with *MultiLinear* material, and b) force-displacement hysteresis curves for the four *twoNodeLink* elements with *BoucWen* material, for one selected recording of IML #5 (T_R = 500 yr).

With reference to the same selected recording of IML #5 considered in Figure 6a, Figure 6b shows the dynamic response of the four *twoNodeLink* elements with *BoucWen* material representing the Resilio hysteretic devices, in terms of force-displacement (hysteresis) curves. First, it is evident how the seismic action pushes the devices to barely exceed a displacement of 0.01 m and a force of 10 kN, these values being quite far from the capacities and the failure condition (see Figure 4b), as expected, given the medium intensity of the selected recording. From the

axial displacement and force time-histories, not shown here due to space constraints, it is observed that the correspondent devices in the two perimeter portal frames along the longitudinal direction experience the same seismic demand, thus reassuring on the regularity in plan of the building and the absence of a torsional behaviour. Also, in each of the two pairs of devices, when one of them is tensioned, the other one is compressed, as expected. Similar to what observed for the friction dampers, the width of the hysteresis loops provides evidence of the energy dissipation occurring due to hysteretic damping.

As already mentioned in Section 1, the dynamic response was assessed with reference to two limit states, namely UPD and GC. The UPD limit state was supposed to be attained as soon as one of two capacity thresholds is first reached. The first one entails a column drift of 1% (RINTC, 2015-2021) [31], actually reduced to 0.5% in consistence with NTC18 (2018) [32] code provisions for RC framed structures with brittle masonry infills. The second threshold deals with a relative displacement of beam-to-column connections that equals 10% of half of the size of the column section, in both directions [19]. On the other hand, the GC limit state was supposed to be attained as soon as it is first reached one of two conditions, namely a column drift causing a 50% drop in base shear following the peak point, in the degrading branch of the pushover curve [31], and half of the size of the column section, in both directions [19]; in fact, attaining the second condition indicates loss of support, with one end of at least one beam in the model falling from its seating.

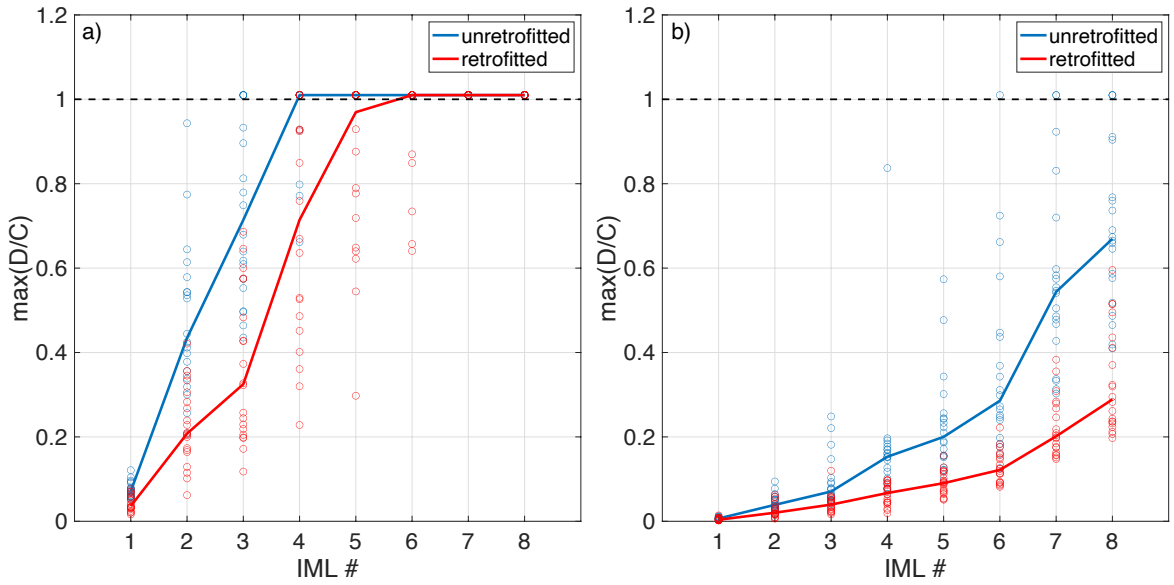

Figure 7: D/C ratio points and median curves obtained via MSA for both the unretrofitted and retrofitted models, at the a) UPD limit state, and b) GC limit state.

Figure 7 displays the demand-over-capacity (D/C) ratio points resulting from MSA, related to both the unretrofitted and retrofitted models, at both limit states. The circles represent the highest D/C ratios, limited to 1, obtained among the two horizontal directions and the two EDPs evaluated, resulting from the 20 NDAs carried out for each of the eight IM levels considered. The median curves are also displayed. These plots allow readily i) observing how the distributions of D/C ratios are correctly dragged towards the capacity line (i.e. D/C = 1) for higher intensity levels, with the median curves monotonically increasing, and ii) checking if any "failure" (i.e. D = C) cases occurred at the generic stripe. More importantly, the plots show a significant reduction of seismic demands for the retrofitted model at both limit states. In particular, at the GC limit state it can be noted how the divergence of the median curves increases with

seismic intensity, reflecting an increase in energy dissipation, as expected. Still with reference to the GC limit state, while the unretrofitted model experienced several failure cases at the highest stripes, for the retrofitted model the capacity was never reached, even at the last (eighth) intensity level, where the median curve drops from about 0.7 to 0.3. Overall, these results do provide reassurance on the efficacy of the proposed dissipation-based retrofitting solutions in effectively yielding a performance enhancement for the case study at hand.

5 CONCLUSIONS

The seismic response of reinforced concrete precast industrial buildings can be generally improved by imposing the dissipation of an appropriate amount of energy. This imparted momentum to research aimed at investigating the effectiveness of energy dissipation devices in enhancing the seismic performance and possibly extending the nominal service life of these structures. Seismic retrofitting with two dissipation devices was considered herein, namely a friction rotation damper and a bracing system with dissipative sacrificial elements. Two three-dimensional numerical models of a case study building representative of the Italian building stock in the ‘70s, with and without the retrofit, were created in OpenSees and firstly subjected to static (pushover) analyses. Then, a dedicated toolbox was employed to select both horizontal components of 20 natural spectrum-compatible recordings, scaled at eight increasing levels of AvgSa, according to the exact CS method. Nonlinear dynamic analyses in both the main directions were undertaken within a multiple-stripe analysis framework.

The obtained results in terms of pushover curves clearly highlighted that the installation of the two dissipation devices coupled with steel profiles preventing joint sliding, leads to a relevant increase in lateral stiffness and resistance along both the main directions. On the other hand, the dynamic analyses results allowed gaining insight into the dynamic behaviour and dissipation capabilities of the two employed devices, thus lending valuable reassurance on the accuracy of the modelling effort in OpenSees. The demand-over-capacity ratio curves at two limit states showed a substantial reduction of seismic demands in terms of column drift with respect to the unretrofitted model, something that was expected and further confirmed the efficacy of the proposed solutions in enhancing the seismic performance of existing and new precast industrial buildings. Ongoing work by the authors is heading towards a quantitative evaluation of i) the life cycle environmental impact of dissipation devices with dry installation, as well as ii) their beneficial effects to the life cycle seismic performance of precast structures. Traditional retrofitting solutions will be modelled as well, to allow for a comparative evaluation of both seismic performance and environmental impact.

ACKNOWLEDGEMENTS

The study presented in this article was developed within the activities of the EUCENTRE-DPC 2022-2024 research program, which was funded by the Presidency of the Council of Ministers - Italian Civil Protection Department (DPC). The authors are also particularly grateful to Dr. Gianfranco Gramola for kindly providing drawings and test results about the Resilio system considered in this work.

REFERENCES

[1] L. Praticò, M. Bovo, N. Buratti, M. Savoia, Large-scale seismic damage scenario assessment of precast buildings after the May 2012 Emilia earthquake. *Bulletin of Earthquake Engineering*, **20**(15), 8411-8444, 2022.

[2] A. Belleri, P. Riva, D. Bolognini, R. Nascimbene, Metodi di protezione sismica di strutture prefabbricate mediante dispositivi di dissipazione. *18° Congresso CTE*, Brescia, Italy, November 11-13, 2010 (in Italian).

[3] P. Martinelli, M.G. Mulas, An innovative passive control technique for industrial precast frames. *Engineering Structures*, **32**(4), 1123-1132, 2010.

[4] S. Santagati, D. Bellotti, D. Bolognini, E. Brunesi, Seismic Response Comparisons between RC Precast Structures with Dissipation Devices on Beam-Column Connections. *15WCEE 2012*, *15th World Conference on Earthquake Engineering*, Lisbon, Portugal, September 24-28, 2012.

[5] A.V. Pollini, C. Mazzotti, M. Savoia, Comportamento sperimentale e numerico di un sistema dissipativo per le connessioni di strutture prefabbricate. *XV Convegno ANIDIS*, Padova, Italy, June 30 - July 4, 2013 (in Italian).

[6] A. Belleri, A. Marini, P. Riva, R. Nascimbene, Dissipating and re-centring devices for portal-frame precast structures. *Engineering Structures*, **15**, 736-745, 2017.

[7] G. Magliulo, M. Cimmino, M. Ercolino, G. Manfredi, Cyclic shear tests on RC precast beam-to-column connections retrofitted with a three-hinged steel device. *Bulletin of Earthquake Engineering*, **15**(9), 3797-3817, 2017.

[8] G. Hu, W. Huang, H. Xie, Mechanical behavior of a replaceable energy dissipation device for precast concrete beam-column connections. *Journal of Constructional Steel Research*, **164**, 105816, 2020.

[9] A. Belleri, S. Labò, Displacement-based design of precast hinged portal frames with additional dissipating devices at beam-to-column joints. *Bulletin of Earthquake Engineering*, **19**(12), 5161-5190, 2021.

[10] J. Bai, J. He, C. Li, S. Jin, H. Yang, Experimental investigation on the seismic performance of a novel damage-control replaceable RC beam-to-column joint. *Engineering Structures*, **267**, 114692, 2022.

[11] V. Quaglini, C. Pettorruso, E. Bruschi, L. Mari, Experimental and Numerical Investigation of a Dissipative Connection for the Seismic Retrofit of Precast RC Industrial Sheds. *Geosciences*, **12**(1), 25, 2022.

[12] D. Sonda, A.V. Pollini, TH Analyses and Simplified Approach for Precast RC Frames Retrofit with Dissipative Fuse Devices Sismocell. *Procedia Structural Integrity*, **44**, 1188-1195, 2023.

[13] B. Dal Lago, M. Naveed, M. Lamperti Tornaghi, Tension-only ideal dissipative bracing for the seismic retrofit of precast industrial buildings. *Bulletin of Earthquake Engineering*, **19**(11), 4503-4532, 2021.

[14] F. McKenna, G.L. Fenves, M.H. Scott, OpenSees: Open System for Earthquake Engineering Simulation. Software tool, University of California, Berkeley, USA, 2000. Available at: http://opensees.berkeley.edu (last accessed 24 February 2023).

[15] F. Jalayer, C.A. Cornell, Alternative non-linear demand estimation methods for probability-based seismic assessments. *Earthquake Engineering & Structural Dynamics*, **38**(8), 951-972, 2009.

[16] N. Jayaram, T. Lin, J.W. Baker, A computationally efficient ground-motion selection algorithm for matching a target response spectrum mean and variance. *Earthquake Spectra*, **27**(3), 797-815, 2011.

[17] L. Luzi, G. Lanzano, C. Felicetta, M.C. D'Amico, E. Russo, S. Sgobba, F. Pacor, ORFEUS Working Group 5, Engineering Strong Motion Database (ESM) (Version 2.0). Ground motion database, Istituto Nazionale di Geofisica e Vulcanologia (INGV), 2020. Available at: https://doi.org/10.13127/ESM.2 (last accessed 24 February 2023).

[18] Resilio system. Patent, Engineering company Astico Brenta, Thiene (Vicenza), Italy, 2017. Available at: https://www.sistemiresilienti.it/resilio-la-differenza/ (in Italian) (last accessed 24 February 2023).

[19] M. Bosio, C. Di Salvatore, D. Bellotti, L. Capacci, A. Belleri, V. Piccolo, F. Cavalieri, B. Dal Lago, P. Riva, G. Magliulo, R. Nascimbene, F. Biondini, Modelling and Seismic Response Analysis of Non-residential Single-storey Existing Precast Buildings in Italy. *Journal of Earthquake Engineering*, **27**(4), 1047-1068, 2023.

[20] G. Magliulo, V. Capozzi, G. Fabbrocino, G. Manfredi, Neoprene–concrete friction relationships for seismic assessment of existing precast buildings. *Engineering Structures*, **33**(2), 532-538, 2011.

[21] L. Liberatore, F. Noto, F. Mollaioli, P. Franchin, In-plane response of masonry infill walls: Comprehensive experimentally-based equivalent strut model for deterministic and probabilistic analysis. *Engineering Structures*, **167**, 533-548, 2018.

[22] B.G. Morgen, Y.C. Kurama, Seismic response evaluation of posttensioned precast concrete frames with friction dampers. *Journal of Structural Engineering*, **134**(1), 132-145, 2008.

[23] S. Bagheri, M. Barghian, F. Saieri, A. Farzinfar, U-shaped metallic-yielding damper in building structures: Seismic behavior and comparison with a friction damper. *Structures*, **3**, 163-171, 2015.

[24] M. Kohrangi, P. Bazzurro, D. Vamvatsikos, A. Spillatura, Conditional spectrum-based ground motion record selection using average spectral acceleration. *Earthquake Engineering & Structural Dynamics*, **46**(10), 1667-1685, 2017.

[25] V. Ozsarac, EzGM, Toolbox for ground motion processing and CS-based selection. Software tool, 2020. Available at: https://github.com/volkanozsarac/EzGM.git (last accessed 24 February 2023).

[26] V. Ozsarac, R. Monteiro, G.M. Calvi, Probabilistic seismic assessment of reinforced concrete bridges using simulated records. *Structure and Infrastructure Engineering*, **19**(4), 554-574, 2021.

[27] M. Pagani, D. Monelli, G. Weatherill, L. Danciu, H. Crowley, V. Silva, P. Henshaw, L. Butler, M. Nastasi, L. Panzeri, M. Simionato, D. Vigano, OpenQuake engine: An open hazard (and risk) software for the global earthquake model. *Seismological Research Letters*, **85**(3), 692-702, 2014.

[28] D.M. Boore, J.P. Stewart, E. Seyhan, G.M. Atkinson, NGA-West2 equations for predicting PGA, PGV, and 5% damped PSA for shallow crustal earthquakes. *Earthquake Spectra*, **30**(3), 1057-1085, 2014.

[29] J.W. Baker, N. Jayaram, Correlation of Spectral Acceleration Values from NGA Ground Motion Models. *Earthquake Spectra*, **24**(1), 299-317, 2008.

[30] CEN EN 1998-1:2004. Eurocode 8: design of structures for earthquake resistance - Part 1: general rules, seismic actions and rules for buildings. European Committee for Standardization, 2004.

[31] RINTC. Implicit seismic risk of code-conforming structures in Italy. *Joint project*, ReLUIS and EUCENTRE, funded by the Italian Department of Civil Protection (DPC), 2015-2021.

[32] NTC18. Aggiornamento delle "Norme tecniche per le costruzioni". Decreto Ministeriale del 17/01/2018. Suppl. ord. n. 8 alla G.U. n. 42 del 20/02/2018 (in Italian), 2018.